Supplementary Information (SI) for Journal of Materials Chemistry A.

Electronic Supplementary Information

In-situ Growth of Sulfur-incorporating NiCo-LDH for a High-Performance Hybrid All-Solid-State Supercapacitor

Sudhir Kumar and Debabrata Pradhan*

Materials Science Centre, Indian Institute of Technology, Kharagpur 721 302, W. B., India

*Email: deb@matsc.iitkgp.ac.in

Materials Characterization

The crystal structure and phase analysis of the synthesized materials were carried out by powder X-ray diffraction (Malvern Panalytical-Empyrean diffractometer) operated at 40 mA and 45 kV with 2θ scan using Ni-filtered Cu K_α X-ray (λ = 1.54 Å) in reflection geometry, equipped with a position sensitive detector. The bonding information of the synthesized materials was studied by using a T64000 Raman spectrometer (Jobin Yvon Horiba, France). The functional groups of the materials were studied using Fourier-Transform Infrared (FTIR-Spectrophotometer, NICOLET 6700). The surface elemental and atomic oxidation states were analyzed with X-ray photoelectron spectroscopy (XPS, PHI 500 Versa Probe II) with a monochromatic Al Kα X-ray source (1486.6 eV). The surface morphology of all the prepared materials was examined using a field emission scanning electron microscope (FESEM, Zeiss, Gemini 500), and the elemental distribution in the materials was obtained using energy dispersive spectroscopy (EDS). The microstructure of the materials was analyzed by using a high-resolution transmission electron microscope (HRTEM). The surface area and pore sizes were estimated by Brunauer-Emmett-Teller (BET) analysis with an Autosorb iQ2 volumetric physisorption analyzer (Quantachrome, ChemBET analyzer) using N_2 adsorption-desorption isotherms at 77 K.

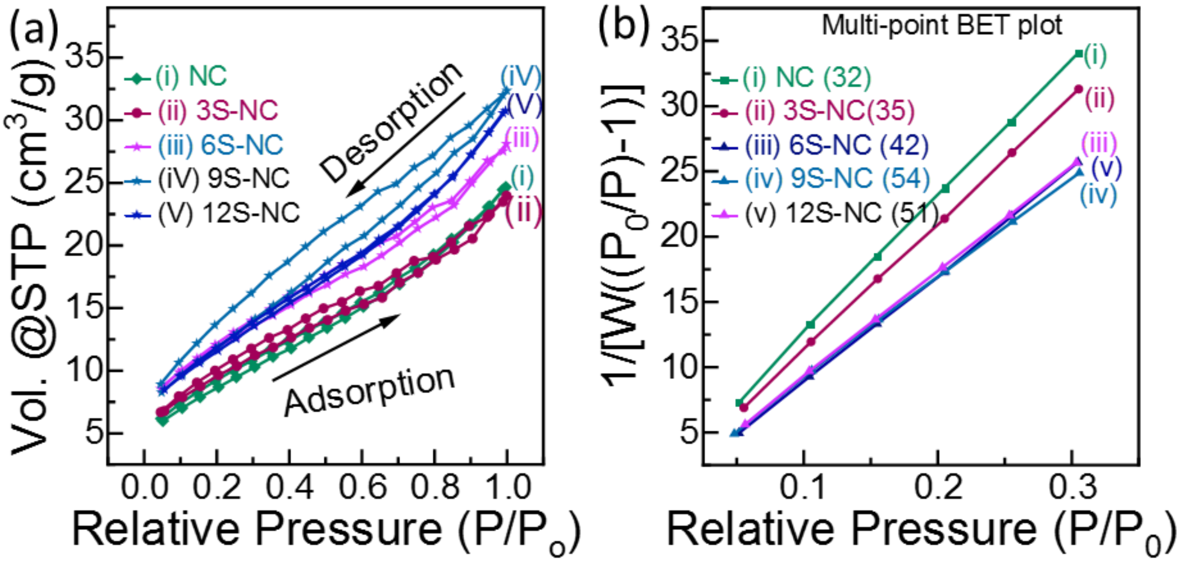

Fig. S1. (a) BET N_2 adsorption-desorption loops, and (b) Multi-point BET plot of the NC, 3S-NC, 6S-NC, 9S-NC, and 12S-NC powder sample obtained during in-situ growth of NiCo-LDHs.

Table S1. BET analysis results of NC, 3S-NC, 6S-NC, 9S-NC, and 12S-NC.

Sample	Surface area (m^2/g)	Pore vol. (cc/g)	Pore radius (A^o)
NC	32	0.05	14.2
3S-NC	35	0.052	14.6
6S-NC	42	0.05	15.1
9S-NC	54	0.056	15.4
12S-NC	51	0.055	15.3

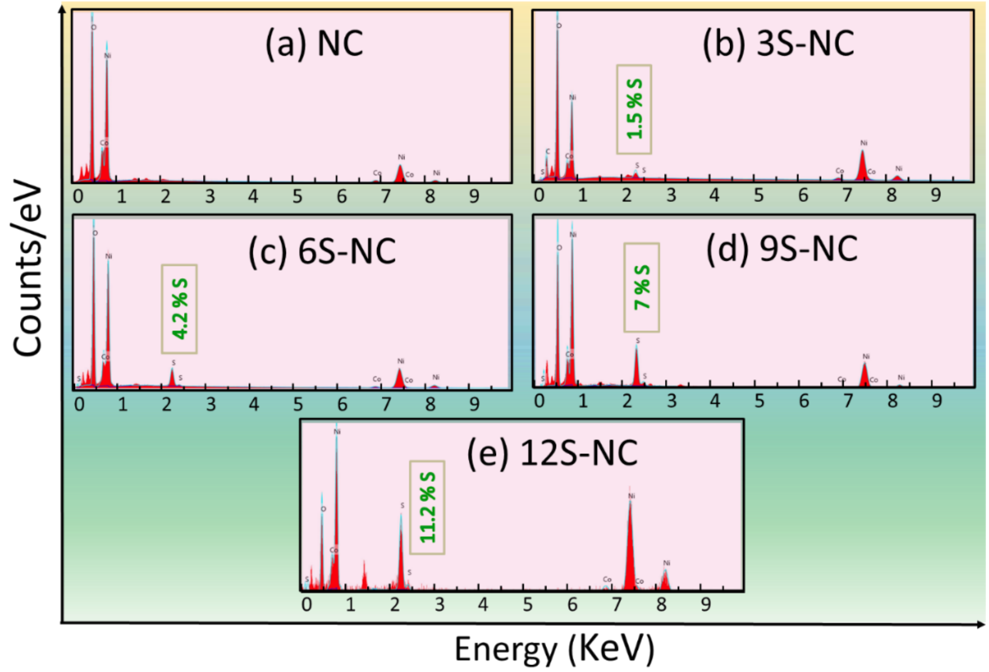

Fig. S2. The EDAX spectrum of (a) NC, (b) 3S-NC, (c) 6S-NC, (d) 9S-NC, and (e) 12S-NC.

Table S2. Atomic percentage of Ni, Co, O, and S in the NC, 3S-NC, 6S-NC, 9S-NC, and 12S-NC samples.

Sample	Ni	Co	O	**S**
NC	35	11	54	
3S-NC	29	8.5	61	1.5
6S-NC	31	10.3	54.5	4.2
9S-NC	37	9	47	7
12S-NC	54	7.8	27	11.2

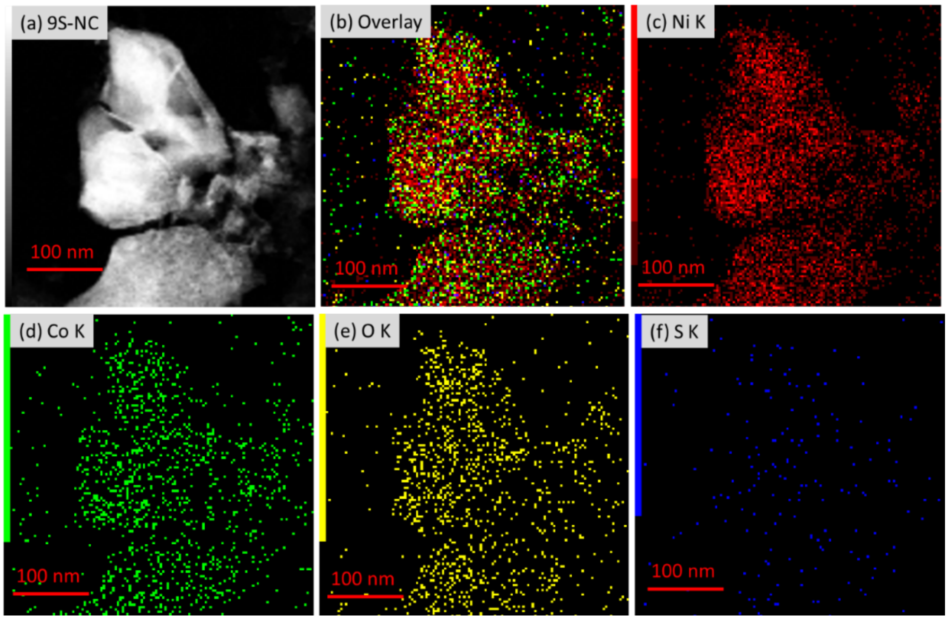

Fig. S3. (a) HAADF-STEM image of 9S-NC nanosheets, HAADF-STEM EDX mapping (b) all element overlay, and specific elemental distributions of (c) Ni K, (d) Co K, (e) O K, and (f) S K.

XPS Analysis of 12S-NC

Fig. S3a shows the presence of Ni, Co, O, C, and S in the survey spectrum of 12S-NC. In the S 2p region XPS spectrum (Fig. S3b), the major deconvoluted peaks at 161.6 and 162.9 eV correspond to S $2p_{3/2}$ and S $2p_{1/2}$ with a binding energy difference of 1.3 eV, which reveals the metal–sulfur (Ni−S and Co−S) bonding.[1,2] Additionally, the minor deconvoluted peaks at 167.9 and 169.2 eV correspond to S $2p_{3/2}$ and S $2p_{1/2}$ with a binding energy difference of 1.3 eV, which reveals the sulfite species (SO_3^{2-}).[3,4] The notable peak of Ni/Co–S suggests a higher proportion of sulfide than sulfite in the 12S-NC sample, in contrast to the results in the 9S-NC sample. This evidence indicates that the phase transformation from sulfite to sulfide occurs upon increasing the sulfur precursor in the synthesis. The chemical oxidation states of nickel are represented as Ni^{2+} and Ni^{3+}, while cobalt exhibits similar oxidation states of Co^{2+} and Co^{3+}, as illustrated in Fig. S3c,d. The bonding characteristics of oxygen and carbon are analogous to those of 9S-NC, as illustrated in Fig. S3e,f.

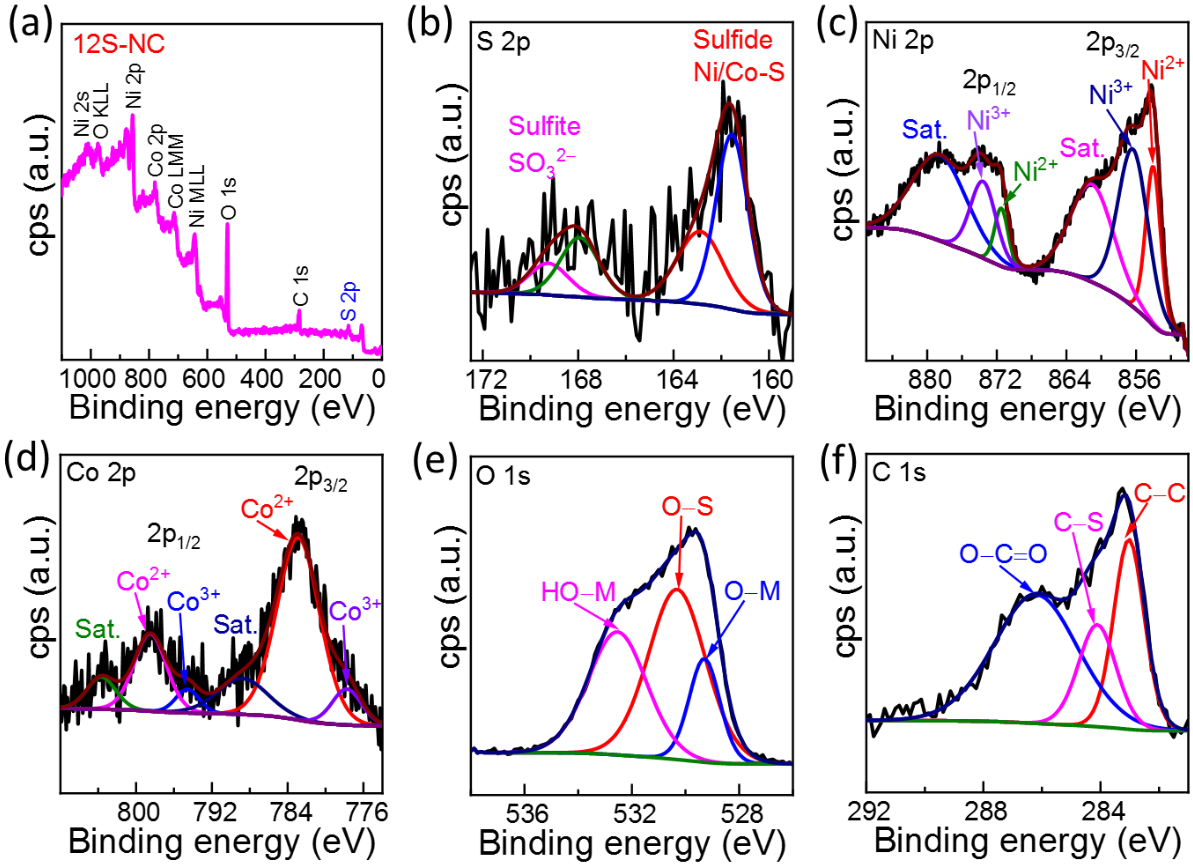

Fig. S4. (a) Survey XPS spectrum of 12S-NC. High-resolution XPS spectra of (b) S 2p, (c) Ni 2p, (d) Co 2p, (e) O 1s, and (f) C 1s of 12S-NC.

PVA-KOH Gel Synthesis

To prepare PVA-KOH polymeric electrolyte gel, 0.5 g of PVA was poured into 10 mL of Millipore water in a 50 mL beaker and placed on a stirrer hot plate at 80 °C for three hours to dissolve completely. Then, 2.5 g of KOH was added to 10 mL of Millipore water. Both the preceding solutions were mixed under stirring at 80 °C. The final solution was agitated at 80 °C for 30 min and then cooled to room temperature to get the PVA-KOH gel.

Electrochemical Study

The electrochemical performance of all the synthesized materials was measured in a three-electrode configuration in 2 M KOH aqueous solution, where a saturated calomel electrode (SCE), a graphite rod (GR), and the fabricated electrode served as the reference, counter, and working electrode, respectively. The energy storage capability of the synthesized materials was measured from cyclic voltammetry (CV), galvanostatic charge-discharge (GCD), and electrochemical impedance spectroscopy (EIS) techniques using a CHI7091E electrochemical workstation (CH Instruments, Inc., USA).

Table S3. Weight of the active materials grown on Ni−foam.

Sample	Ni−foam weight (mg)	After growth weight (mg)	Weight of active materials growth (mg)
NC	55.2	57.4	2.2
3S-NC	56.5	58.9	2.4
6S-NC	55.7	58.5	2.8
9S-NC	57.1	59.6	2.5
12S-NC	56.2	58.8	2.6

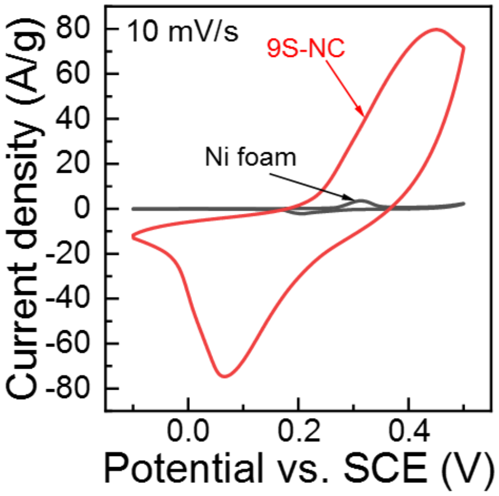

Fig. S5. CV curve of Ni foam and 9S-NC at 10 mV/s scan rate.

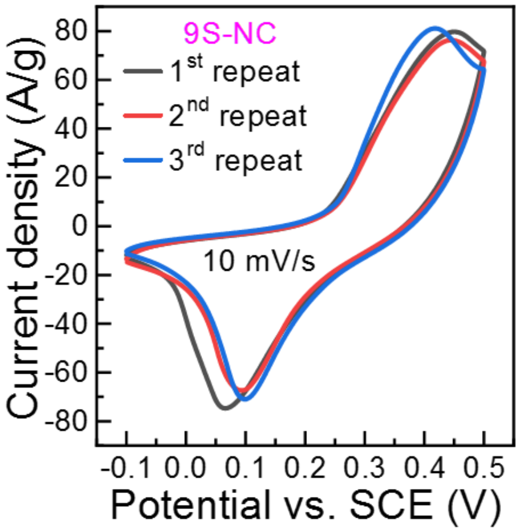

Fig. S6. CV curves of three repeated prepared samples 9S-NC at a 10 mV/s scan rate.

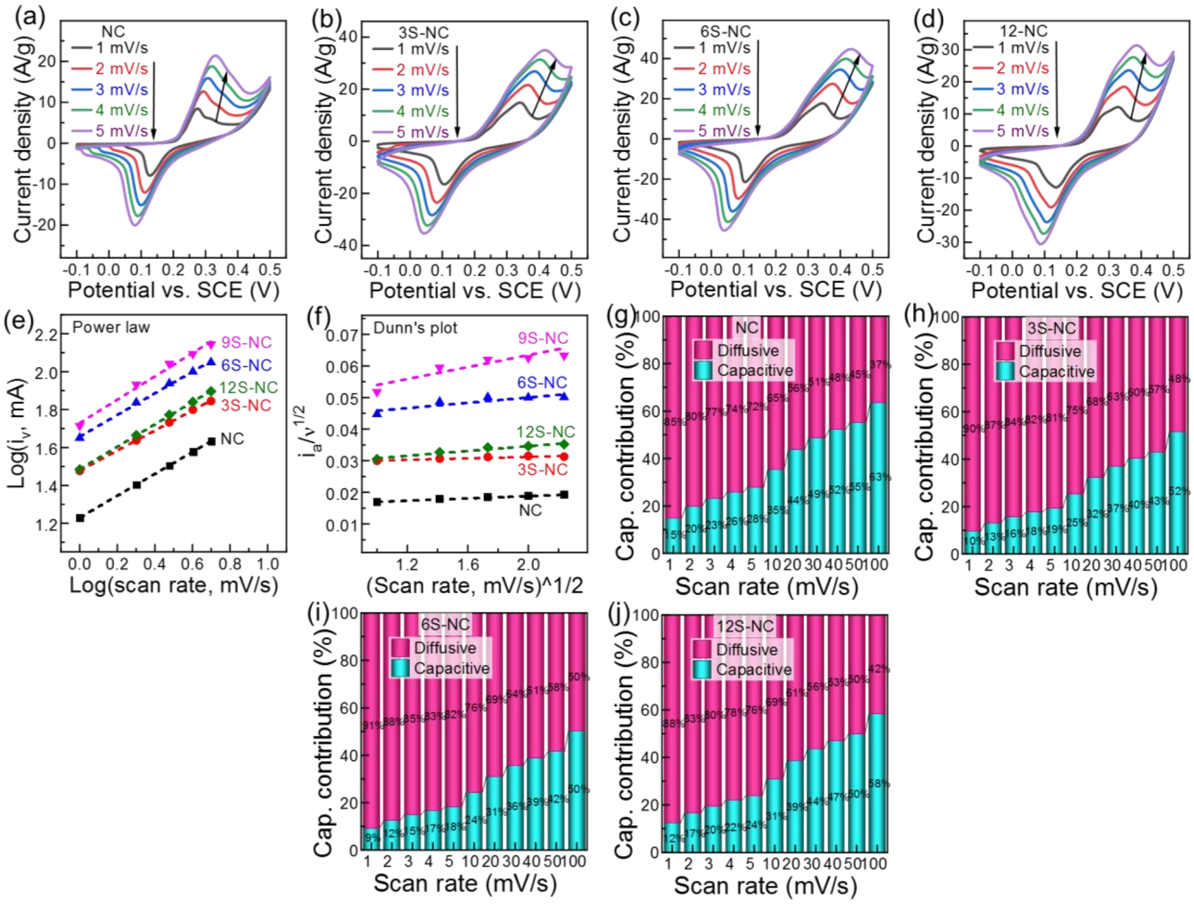

Fig. S7. CV curves of (a) NC, (b) 3S-NC, (c) 6S-NC, and (d) 12S-NC at various scan rates (1−5 mV/s). (e) Linear plot of log (scan rate) vs. log (peak current), (f) linear plot of (scan rate)$^{1/2}$ vs. [peak current/(scan rate)$^{1/2}$)]. The capacitive and diffusive capacitance contribution of (g) NC, (h) 3S-NC, (i) 6S-NC, and (j) 12S-NC at various scan rates.

Table S4. Capacitance contribution measurement parameters.

Sample	b	k_1	k_2
NC	0.65	0.0026	0.015
3S-NC	0.53	0.0012	0.029
6S-NC	0.57	0.0042	0.042
9S-NC	0.6	0.007	0.048
12S-NC	0.59	0.0038	0.027

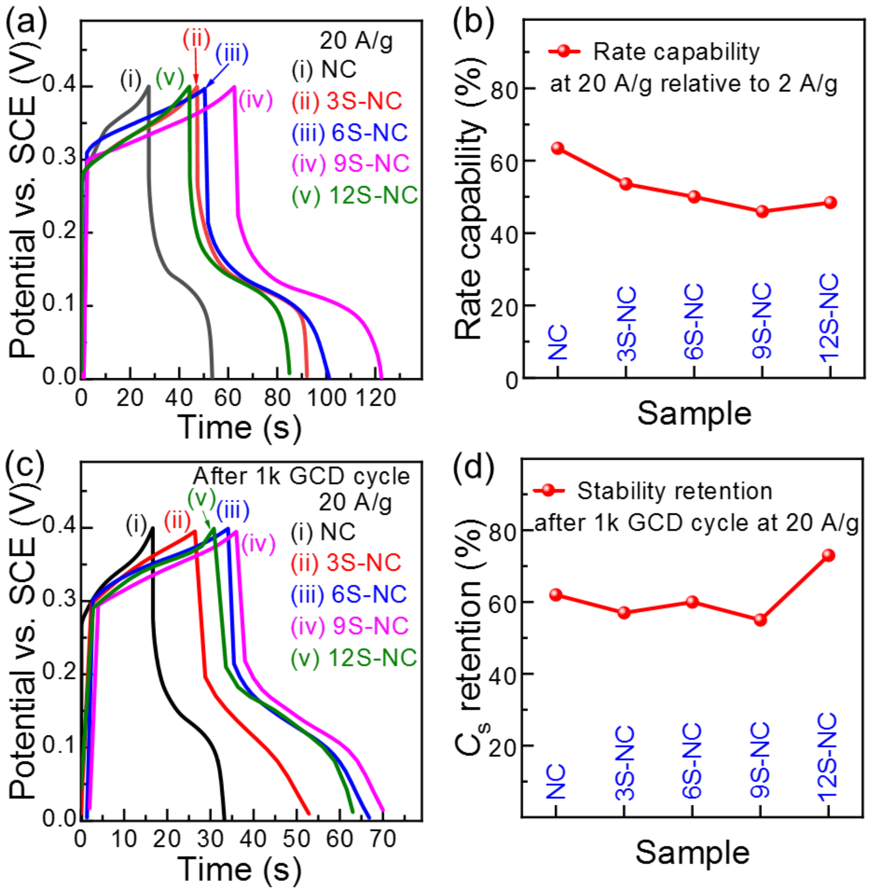

Fig. S8. (a) GCD curves, (b) rate capability plot, (c) GCD curves after 1000 GCD cycles, and (d) stability retention at 20 A/g current density for all the as-prepared samples.

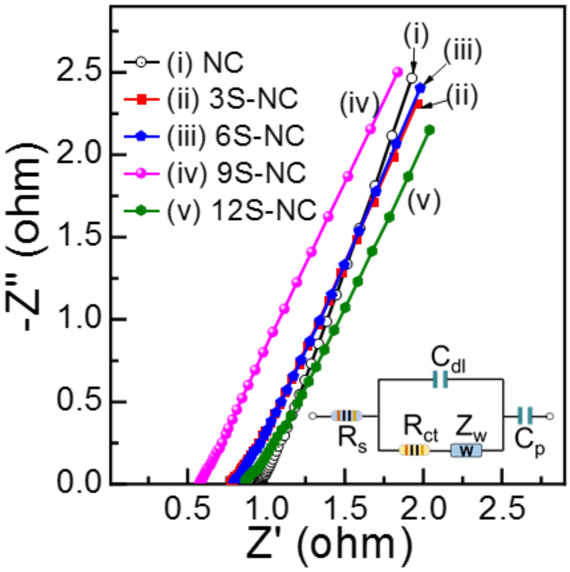

Fig. S9. Nyquist plots of the prepared electrode samples.

Table S5. The EIS analysis of the NC, 3S-NC, 6S-NC, 9S-NC, and 12S-NC samples.

Sample	R_s (Ω)	R_{ct} (Ω)	Z (Ω)
NC	0.95	0.05	2.6
3S-NC	0.78	0.042	2.1
6S-NC	0.79	0.04	2.1
9S-NC	0.58	0.032	1.98
12S-NC	0.86	0.08	1.86

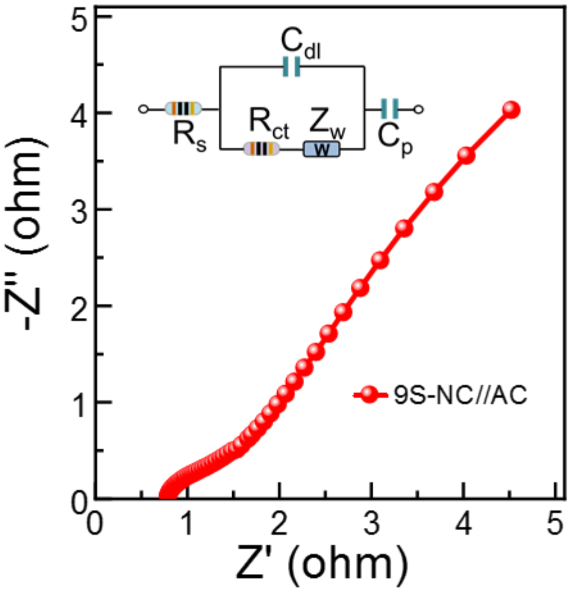

Fig. S10. The Nyquist plot of aq. 9S-NC//AC HSC device.

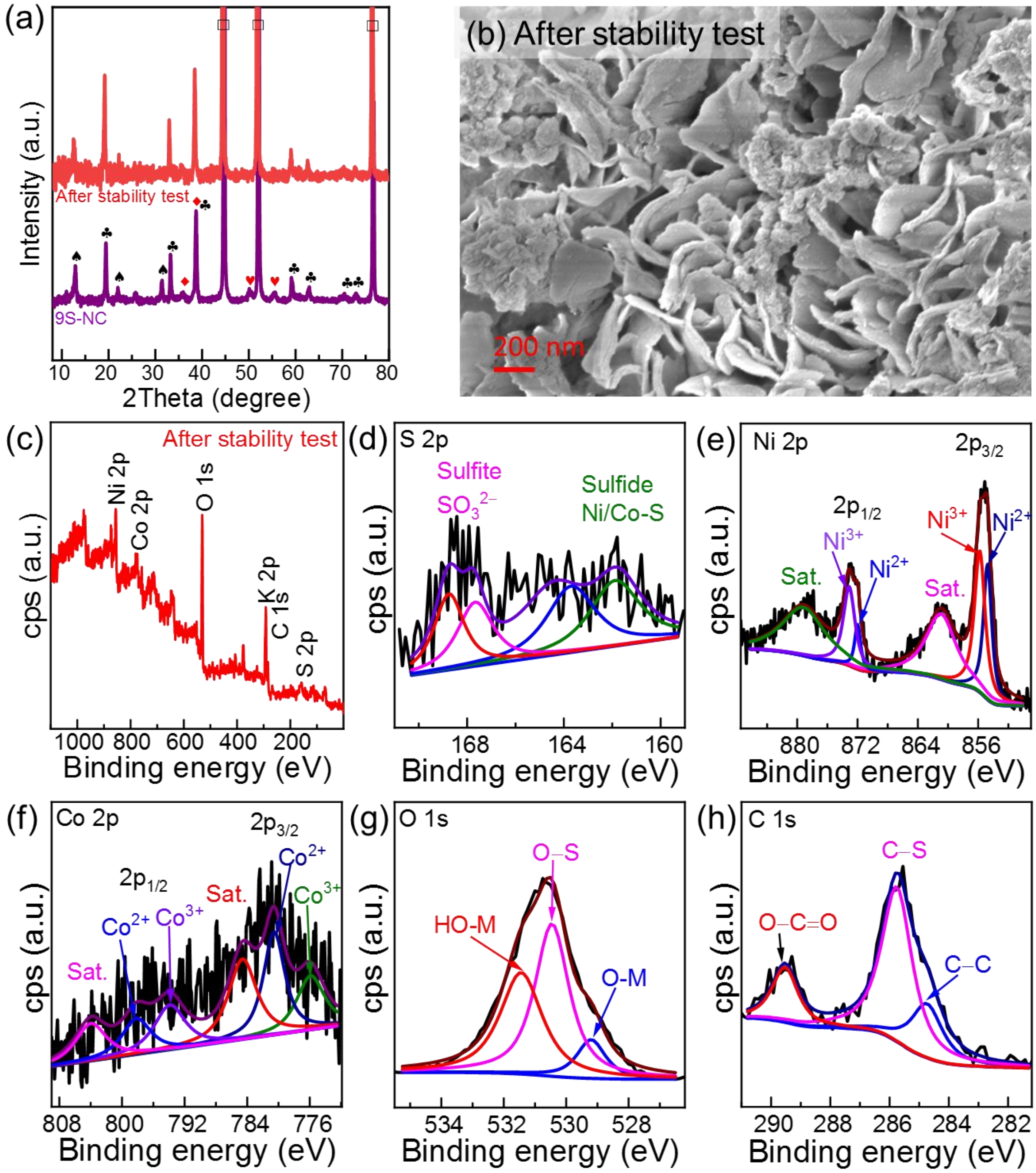

Fig. S11. (a) XRD patterns. The diffraction peaks marked with ♣ and ♦ symbols are assigned to $Ni(OH)_2$ and $Co(OH)_2$, respectively. The peaks marked with ♠ are for the sulfite phase. (b) FESEM image, and (c) XPS survey spectrum of the 9S-NC after stability test. High-resolution XPS spectra of (d) S 2p, (e) Ni 2p, (f) Co 2p, (g) O 1s, and (h) C 1s collected from the NiCo-LDH electrode after the cycling stability test to analyze the elemental composition and oxidation states.

Video: LED light illuminating, calculator powering, and fan running video by aqueous and solid-state fabricated device of 9S-NC//AC HSC.

References

1. X. Tian, M. Xue, Y. Cheng, L. Che, M. Liu, N. B. S. Selabi and Y. Zhou, *Mater. Des.* 2023, **237**, 112598.
2. R. Karthikeyan, D. Thangaraju, N. Prakash and Y. Hayakawa, *CrystEngComm* 2015, **17**, 5431-5439.
3. H. Wang, X. Qiu, W. Wang, L. Jiang and H. Liu, *Front. Chem.* 2019, **7**, 855.
4. K. S. Kim, N. M. Shinde, J. M. Yun and K. H. Kim, *RSC Adv.* 2021, **11**, 12449-12459.